Collective relaxation dynamics and crystallization kinetics of the amorphous Biclotymol antiseptic

*Pragya Tripathi, Michela Romanini, Josep Lluis Tamarit, and Roberto Macovez**

Grup de Caracterització de Materials, Departament de Física i Enginyieria Nuclear, ETSEIB, Universitat Politècnica de Catalunya, Av. Diagonal 647, E-08028 Barcelona, Spain

* Corresponding author: roberto.macovez@upc.edu

Abstract

We employ dielectric spectroscopy to monitor the relaxation dynamics and crystallization kinetics of the Biclotymol antiseptic in its amorphous phase. The glass transition temperature of the material as determined by dielectric spectroscopy is T_g = 290±1 K. The primary (α) relaxation dynamics is observed to follow a Vogel–Fulcher–Tammann temperature dependence, with a kinetic fragility index *m* = 86±13, which classifies Biclotymol as a relatively fragile glass former. A secondary relaxation is also observed, corresponding to an intramolecular dynamic process of the non-rigid Biclotymol molecule. The crystallization kinetics, measured at four different temperatures above the glass transition temperature, follows an Avrami behavior with exponent virtually equal to *n* = 2, indicating one-dimensional crystallization into needle-like crystallites, as experimentally observed, with a time-constant nucleation rate. The activation barrier for crystallization is found to be E_a = 115±22 kJ mol^{-1}.

Keywords: Amorphous, Biclotymol, dipolar relaxation, crystallization kinetics, Avrami law, stability

Introduction

Pharmaceutically active molecules and active pharmaceutical ingredients (API's) are generally stored in solid form, either as crystalline or amorphous (glassy) powders. Compared to the crystalline form, the amorphous form of API's offers the advantage of a higher solubility (Gupta *et al*, 2004) and bioavailability (Serajuddin, 1999). The amorphous glass state has however the disadvantage of being thermodynamically unstable against the nucleation of crystalline phases (Bhardwaj *et al*, 2013; Zhou et al, 2002). The microscopic mechanisms governing the kinetic stability of amorphous API remains unclear, and the crystallization kinetics appears to be determined by a large number of factors such as preparation method, thermal and mechanical treatments employed during formulation (Patterson *et al*, 2005), storage temperature, application of pressure or exposure to humidity (Yu, 2001). It is generally found that storage well below the glass transition temperature T_g (*e.g.*, at T_g – 50 K) prevents crystallization of the amorphous state and thus ensures a physically stable drug during its shelf-life (Capen *et al*, 2012; Pogna *et al*, 2015). In general, the thermal energy and the molecular mobility below T_g are considered to be too low to produce the rearrangements necessary for the nucleation of the crystalline phase, although some authors have proposed that the secondary Johari-Goldstein relaxation (considered as the primitive relaxation) can provide enough mobility to activate the crystallization process.(Adrjanowicz *et al*, 2012a) A recent study (Schammé

et al, 2015) on Biclotymol, 2,2”-methylenebis(4-chloro-3methylisopropylphenol), an antiseptic used for mouth, throat and pulmonary infections, has shown that it can be stored in its amorphous form during months also several degrees above the T_g of the material, *i.e.*, at temperatures at which the material is in the supercooled liquid state and the molecular mobility is slow but not negligible. Motivated by this finding, we present here an experimental study of the recrystallization of Biclotymol from its supercooled state at four different temperatures, by means of broadband dielectric spectroscopy, a well-established technique to investigate crystallization kinetics in API's (Adrjanowicz *et al*, 2010; Kaminski *et al*, 2011; Adrjanowicz *et al*, 2012b). We find in particular that crystallization takes place on the timescale of hours even at moderate temperatures (T_g + 14K), and that therefore temperature control is critical to preserve the amorphous state. Moreover, we study in detail the fragility of this glass-forming API and the crystallization mechanism. Crystallization can be well described by the Avrami law with integer exponent *n* equal to 2, corresponding to one-dimensional growth of needle-like crystallites, as experimentally observed, with a time-independent nucleation rate.

Material and methods

Biclotymol powder of medicinal grade was provided by Bouchara-Recordati (France) and used as received. The sample batch was the same as in our previous work (Céolin et al, 2008). Differential scanning calorimetry measurements were carried out in the temperature range between 250 and 450 K with heating or cooling rates 10 K min^{-1}, using a Q100 calorimeter from TA-Instruments. The value of the melting temperature determined by calorimetry was used as a check that the quality of the sample had not deteriorated.

Dielectric measurements were carried out in parallel-plate capacitor configuration with a Novocontrol Alpha analyzer. The sample was initially melted above 400 K and inserted in the molten state inside a home-made stainless steel capacitor specially designed for liquid samples, with plates separated by silica spacers. The capacitor was held at high enough temperature to ensure that the sample remained liquid during the filling, and was then mounted in the dielectric spectroscopy setup. For the measurements of the molecular dynamics (those of Figure 1), 50 µm diameter spacers were used to achieve a higher capacitance, while for isothermal crystallization measurements (Figures 3 and 4) 100 µm diameter spacers were employed, to avoid any effect due to geometrical constraints on the sample. The probed temperature range was between 115 K and 350 K, and dielectric measurements were carried out in the frequency (*f*) range from 10^{-2} to 10^{8} Hz. Most measurements were carried out between 10^{-2} to $5 \cdot 10^{6}$ Hz using a Novocontrol Alpha analyzer. Few measurements were carried out between 10^{6} and 10^{8} Hz to probe the secondary relaxation dynamics above the glass transition temperature. For these high-frequency measurements a HP4291 impedance analyzer was employed in reflectometry geometry, with the sample capacitor mounted at the end of a coaxial cable.

In all measurements, the sample was initially re-melted inside the capacitor and then cooled down as fast as possible to below T_g to avoid crystallization. All measurements of the primary α relaxation were measured while heating up for the same reason, and for isothermal crystallization measurements the measuring temperature was reached by heating as fast as possible from T_g (see

the Results and Discussion Section). Temperature control of the capacitor and thus of the sample was achieved with a nitrogen-gas flow cryostat. The typical maximum heating/cooling rates were not higher than 15 K/minute.

Dielectric spectroscopy yields the complex permittivity ε of the sample as a function of f. Dynamic relaxation processes are visible as broad peaks in the so-called loss spectra (semi-logarithmic plots of the imaginary part of ε"(f) of the complex permittivity), in correspondence of which a step-like decrease is observed in the real part ε'(f) as the real and imaginary parts of ε are related by Kramers-Kronig transformations (Kremer and Schönhals, 2003). Biclotymol exhibited two dynamic processes, namely a collective primary relaxation at lower frequency (α process) and a secondary dynamics at higher frequency. The primary relaxation feature was fitted with a Havriliak–Negami function, superposed to a background proportional to reciprocal frequency that mimicked the conductivity contribution to the loss spectra. The analytic expression of the Havriliak–Negami function is (Havriliak and Negami, 1966; Havriliak and Negami, 1967):

(Eq. 1) $\varepsilon_{HN}(f) = \varepsilon_\infty + \frac{\Delta\varepsilon}{(1+(i2\pi f\tau_{HN})^\beta)^\gamma}$,

where $\Delta\varepsilon = \varepsilon_s - \varepsilon_\infty$ is the dielectric strength (equal to the step variation of ε', and proportional to the density of molecules taking part in the relaxation process), and ε_∞ and ε_s are the high-frequency and static low-frequency limits of the real permittivity. The parameters β and γ, called Havriliak–Negami exponents, lie in the range from 0 to 1 and are related with the shape and asymmetry of the relaxation time distribution; finally, τ_{HN} is a fitting parameter from which the characteristic time τ_α at which the dielectric loss of the primary relaxation process is maximum is obtained as:

(Eq. 2) $\tau_\alpha = \tau_{HN}\left(\sin\frac{\beta\pi}{2+2\gamma}\right)^{-1/\beta}\left(\sin\frac{\beta\gamma\pi}{2+2\gamma}\right)^{1/\beta}$.

The secondary relaxation processes was fitted as a Cole–Cole function, commonly employed for secondary relaxations (Kremer and Schönhals, 2003), which is a special case of the Havriliak–Negami function with $\gamma = 1$. In such case, it may be seen from Eq. (2) that the characteristic relaxation time τ_s of the secondary process is directly the value of the Cole–Cole fit parameter, namely $\tau_s = \tau_{CC} = \tau_{HN}(\gamma = 1)$. For the fit of the spectra of the secondary relaxation, a background proportional to reciprocal frequency was also added, to reproduce the high-frequency tail of the α process.

Results and Discussion

Figure 1 shows the real (a) and imaginary (b) part of the complex relative dielectric permittivity of Biclotymol in its supercooled liquid (amorphous) state, as measured upon heating from low temperature (only the data between T_g and T_g + 32 K are shown; the molecular structure of Biclotymol is shown as an inset to Figure 1(a)). A clear primary relaxation is observed, visible as a peak in the imaginary permittivity (b) and as a corresponding decrease in the real permittivity (a). The primary relaxation corresponds to the so-called α process stemming from the collective reorientation of the Biclotymol molecules. The value of the real part of the permittivity at frequencies lower than the primary relaxation can be taken as an estimate of the relative dielectric constant of the material. For amorphous Biclotymol, it appears to be roughly 6 near room temperature.

As expected, the spectral position of the α feature shifts to lower frequency (longer characteristic times) as the temperature is lowered. This cooperative motion freezes out slightly above 290 K (Figure 1(b)), which is consistent with the glass transition temperature obtained from our calorimetry data, displayed in the inset to Figure 2. As visible in this inset, the calorimetric T_g determined from the inflection point of the specific heat jump is 292.5±0.5 K, in agreement with a recent calorimetry study of the crystallization kinetics (Schammé et al, 2015) which reported a glass-transition temperature T_g = 293 K using the same method. A precise determination of the glass transition temperature by dielectric spectroscopy can be obtained from the fit to the dielectric spectra, as discussed later.

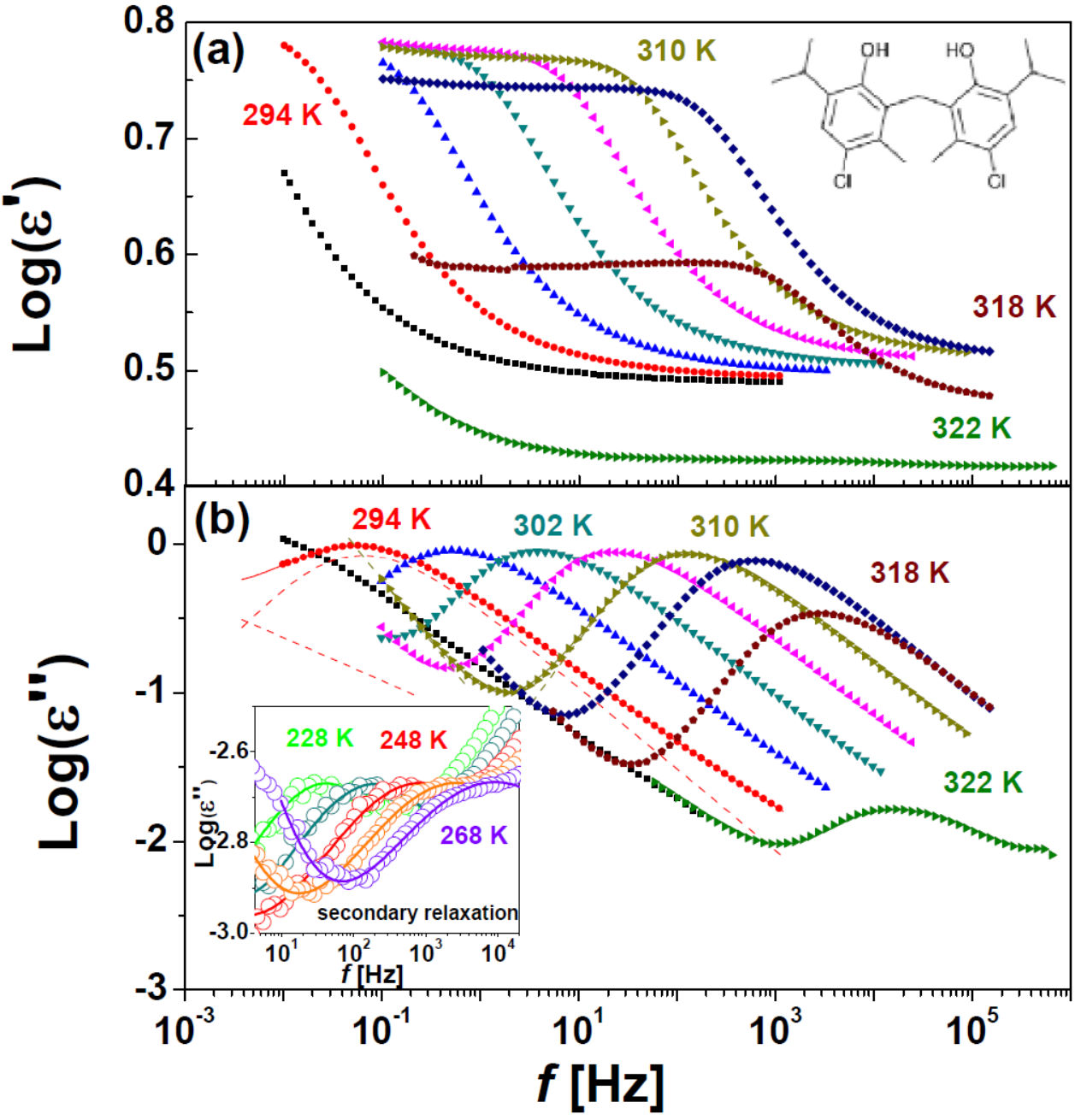

Figure 1. Permittivity spectra ε'(*f*) (a) and loss spectra ε"(*f*) (b) of Biclotymol between 290 and 322 K every 4 K. In (b), continuous lines are fits assuming a Havriliak–Negami profile of the primary α relaxation, on top of a conductivity background proportional to inverse frequency (both contributions are shown as dashed lines). For clarity, the fit results and fit components are displayed only for the temperatures of 294 and 310 K, and only some of the measured spectra are shown. Inset to (a): molecular structure of Biclotymol. Inset to (b): selected loss spectra ε"(*f*) of Biclotymol below T_g (every 10 K between 228 and 268 K), where a secondary relaxation is visible (markers), fitted with a Cole-Cole function plus a background mimicking the high-frequency tail of the α relaxation feature (the fits are displayed as continuous lines).

The sample also exhibited a secondary relaxation feature, visible at higher characteristic frequency than the α process. The inset to Figure 1(b) shows dielectric loss spectra at different temperatures below T_g, to highlight the temperature evolution of the secondary process. It can be observed that the dielectric strength is quite low, namely of the order of 10^{-3} (much smaller than that of the cooperative α relaxation). A high-frequency spectral background, which increases with increasing frequency, may be noticed in these low-temperature spectra. Such high-frequency background could be due to heterogeneities induced in the sample by the rapid cooling to below T_g that was performed to avoid crystallization of the supercooled liquid phase.

For quantitative analysis, the primary and secondary relaxations were fitted assuming a Havriliak–Negami and Cole–Cole lineshape, respectively (see the Material and methods Section). The fit quality may be appreciated in Figure 1(b) both for the loss spectra acquired at 294 and 310 K (main panel) and for the spectra acquired below T_g (inset). A background proportional to inverse frequency (therefore contributing to the low-frequency portion of the spectra) was added in both cases; in the former case, to account for the conductivity contribution and, in the latter case, for the high-frequency wing of the primary feature. From the fit of the experimental data it is possible to extract the values and temperature dependence of the relevant parameters. For the primary relaxation, the exponents of the Havriliak–Negami function were in the range from 0.8 to 0.9 for β and close to 0.55 for γ, although they varied slightly with temperature. For the secondary relaxation, γ was set to unity (Cole-Cole function) and β was in the range between 0.4 and 0.6.

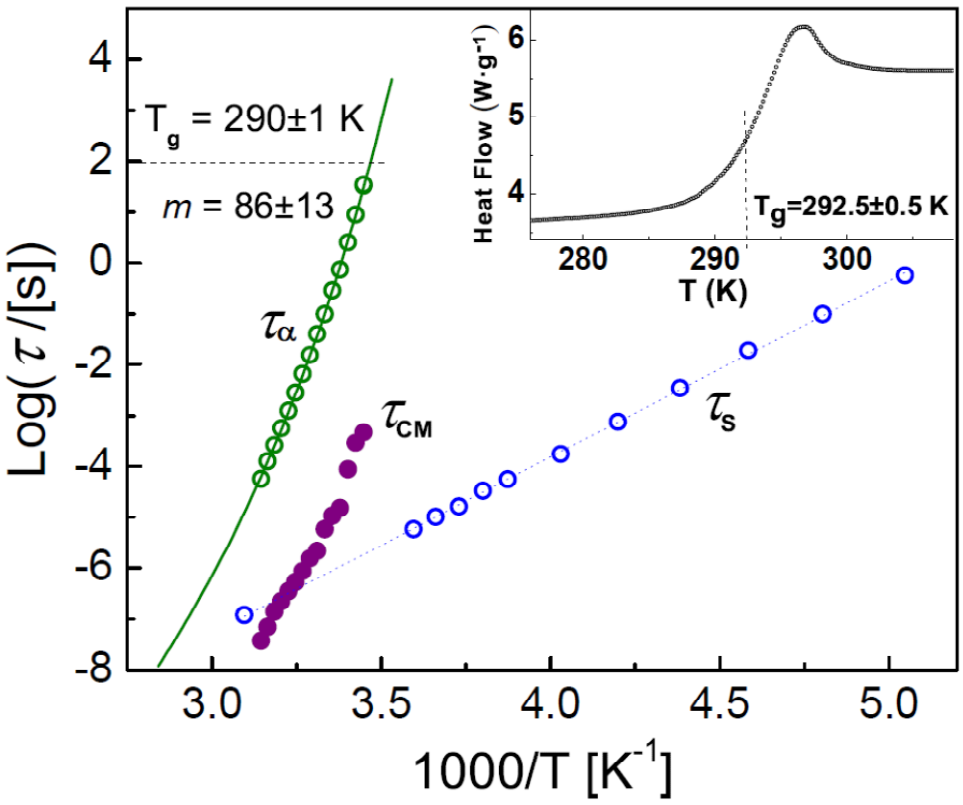

Figure 2. Arrhenius plot of the primary (τ_α) and secondary (τ_s) relaxation times, as extracted from the loss spectra partially displayed in Figure 1(b). The continuous line is the fit of τ_α using the Vogel–Fulcher–Tammann equation (Eq. (3), see the text), while the dotted line is the fit of τ_s assuming a simply-activated (Arrhenius) temperature dependence. The horizontal dashed line indicates the value of τ_α (Log τ_α = 2, *i.e.*, τ_α = 100 s) that corresponds to the glass transition temperature (T_g = 290±1 K). Filled markers indicate the theoretical relaxation time τ_{CM} of a Johari–Goldstein relaxation precursor to the primary relaxation, as calculated according to the Coupling Model (see the text). Inset: differential scanning calorimetry thermogram acquired upon heating from below T_g, after cooling the sample from the molten state at a rate of 10 K min^{-1}. The dashed line indicates the glass transition temperature T_g determined from the inflection point below the endothermic feature in the thermograph.

The relaxation times of both relaxations, τ_α and τ_s (defined in each case as the time of maximum dielectric loss, see the Material and methods Section) are displayed as Arrhenius plots in Figure 2. It is observed that τ_s display a simply activated (Arrhenius) behavior, with constant activation energy E_a = 75.5±0.7 kJ mol^{-1}; instead, τ_α exhibits a more pronounced (super-Arrhenius) temperature dependence. The relaxation time of the α process could be fitted using the so-called modified Vogel–Fulcher–Tammann (VFT) equation (Angell, 1988):

(Eq. 3) $\tau_\alpha = \tau_0 \exp[D\, T_{VF}/(T - T_{VF})]$.

Here the prefactor τ_0, the strength parameter D and the Vogel–Fulcher temperature T_{VF} are phenomenological parameters, whose values obtained from the fit were, respectively, Log(τ_0/[s]) = –18.9 ± 0.9, D = 15.5 ± 1.9 and T_{VF} = 218 ± 4 K. The glass transition temperature, estimated as the temperature at which the VFT function displayed a value of τ_α equal to 100 s, is T_g = 290±1 K, which

matches approximately that estimated by calorimetry. A slight difference between the two techniques might arise due to the different cooling/heating rates in each experiment. A VFT profile is indicative of a cooperative nature of the relaxation process, which becomes more pronounced approaching the glass transition temperature. As it should be in the VFT model, T_{VF} is lower than T_g.

While the α relaxation feature is the collective relaxation process associated with the glass transition, the identification of the secondary process is not as straightforward. Secondary processes in glass forming materials may correspond either to intramolecular motions involving a relative motion of polar sidegroups, or else involve the whole molecule and represent the single-molecule precursor of the cooperative α relaxation. (Kremer and Schönhals, 2003; Ngai and Paluch, 2004) The latter type of secondary relaxations are termed Johari–Goldstein relaxations and are directly correlated with the primary α dynamics (Johari and Goldstein, 1970; Ngai, 1998). For example, according to the so-called Coupling Model (Ngai, 2007), the relaxation time τ_{CM} of the Johari-Goldstein relaxation should be related with that of the primary process (τ_α) as:

(Eq. 4) $\tau_{\mathrm{CM}} = t_c^p(\tau_\alpha)^{1-p}$.

Here t_c is a cross-over time, whose typical value is 2×10^{-12} s for molecular and polymeric glass formers (Colmenero *et al*, 1997; Ngai, 2007), and *p* is a shape parameter of the α relaxation given by $p = 1 - \beta_{KWW}$, where β_{KWW} is the exponent of the stretched exponential function that describes the α spectral feature in the time domain. For the obtained shape parameters (β,γ) of the HN function employed to fit the α relaxation, the value of *p* can be accurately estimated as $p \cong 1 - (\beta\gamma)^{\frac{1}{1.23}}$ (Alvarez *et al*, 1991; Alvarez *et al*, 1993). The theoretical precursor time τ_{CM} calculated using Eq. (4) is shown in Figure 2 together with the experimental values of τ_α and τ_s. It may be observed that τ_s is, for most temperatures, quite far from the value expected for a Johari–Goldstein precursor, and has a totally different temperature dependence, which indicates that the secondary process is an intramolecular relaxation rather than a whole-molecule relaxation. This is also confirmed by the fact that the activation energy (slope) of the secondary relaxation does not change below T_g (see Figure 2), as it is instead customary for Johari-Goldstein relaxations (Ngai, 1998; Capaccioli *et al*, 2007). Judging from its relatively high activation energy (75.5±0.7 kJ mol^{-1}), it is likely that this intramolecular secondary dynamics involves the hydrogen bonds formed by the hydroxyl groups (and possibly the chlorine atoms) of Biclotymol, as found in other organic small-molecule glass formers (Hensel-Bielowka *et al*, 2005), given that hydrogen bonds have a relatively high cleavage energy leading to a high activation energy of associated secondary processes (Macovez *et al*, 2014).

From the fit of τ_α with Eq. (3) one may obtain the kinetic fragility index of the Biclotymol glass-former. The fragility index is defined as:

(Eq. 5) $m = \left.\frac{d(\mathrm{Log}\tau_\alpha)}{d(T_g/T)}\right|_{T=T_g}$

The obtained experimental value is *m* = 86±13. This value matches that calculated directly from the VFT fit parameters listed above according to the relation $m = \frac{D}{\mathrm{Ln}(10)}\frac{T_{VF}/T_g}{(1-T_{VF}/T_g)^2} = 82 \pm 15$ (Böhmer et al, 1993). Both values are slightly lower than (but compatible with) the value obtained from

calorimetry experiments (Schammé et al, 2015), which was reported to be 99±5. This confirms, by means of a more direct experimental tool such as dielectric spectroscopy, that Biclotymol is a rather fragile glass-former (Schammé *et al*, 2015).

As for the temperature dependence of the dielectric strength of the loss feature, it is constant for temperatures close to T_g, while it is observed to decrease upon heating (in Figure 1, starting from 318 K). Since the dielectric strength $\Delta\varepsilon$ is proportional to the number of molecules participating in the cooperative α relaxation, the decrease of the dielectric strength is indicative of a recrystallization process, in which some molecules are removed from the supercooled liquid phase, in which they are mobile, to form crystallites in which all motion ceases.

Crystallization is more likely to take place at higher temperature because the viscosity η, which is essential to the crystallization transition (Ediger *et al*, 2008), is lower the higher the temperature. The molecular diffusional relaxation time τ_α is related to the viscosity by the relation $\eta = G_\infty \tau_\alpha$, where G_∞ is the elastic shear modulus, that does not vary considerably in the supercooled liquid regime (Kremer and Schönhals, 2003). In other words, the relaxation time τ_α of the primary process is basically proportional to the viscosity and thus directly correlated with the crystallization process. Just as the primary relaxation boosts the crystallization transition, it has been suggested that secondary precursor relaxations (Johari–Goldstein) could also trigger crystallization (Adrjanowicz *et al*, 2012a). A partial evidence for this is the fact that glasses are generally stable against crystallization only well below T_g (Capen *et al*, 2012), namely, at temperatures at which not only the primary process, but also precursor secondary relaxations are frozen. As discussed, the secondary relaxation in Biclotymol is not a precursor relaxation but rather an intramolecular one, which would explain why the material is stable against crystallization already near T_g (Schammé *et al*, 2015), where only the α process is almost frozen while the secondary relaxation is not.

To characterize in detail the crystallization from the supercooled liquid state, we performed four separate experiments at four fixed temperatures, which were reached by heating up from a temperature lower than T_g to preserve (initially) the supercooled liquid state. The experimental results are reported in Figures 3 and 4 for the real and imaginary parts of the permittivity, respectively. As already reported in previous studies, the supercooled liquid phase of Biclotymol crystallizes into a metastable solid phase referred to as Phase II (Schammé *et al*, 2015; Ceolin *et al*, 2008), rather than into the stable crystal phase, referred to as Phase I.

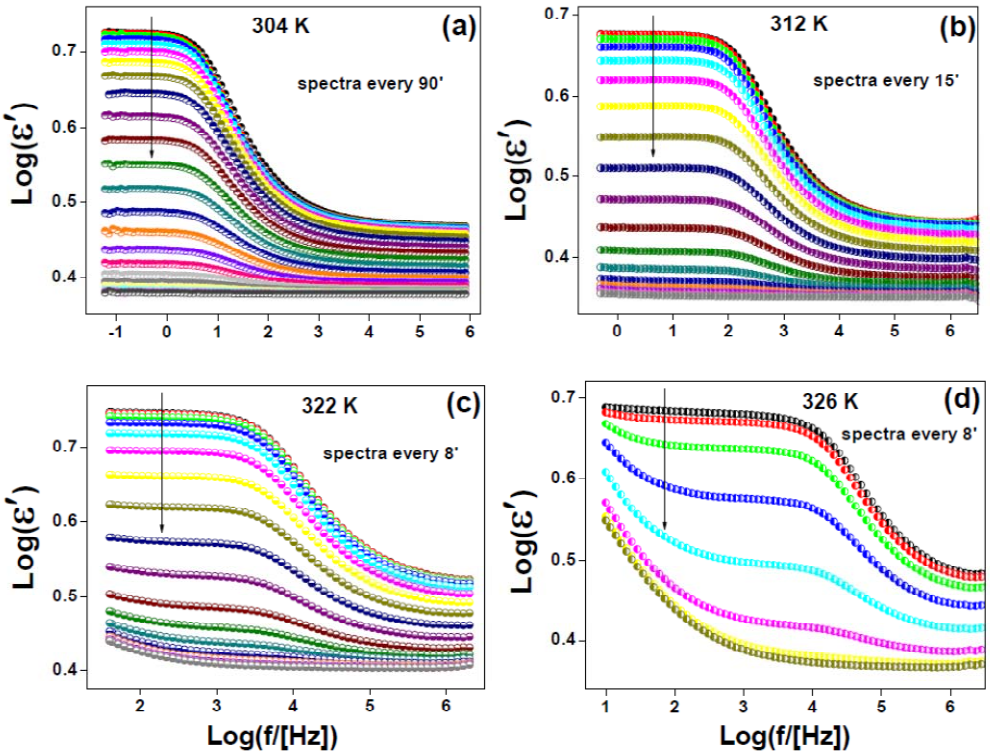

Figure 3. Permittivity spectra ε′(*f*) of Biclotymol during isothermal dielectric measurements at the temperatures of 304 (a), 312 (b), 322 (c) and 326 (d) K. The arrows indicate the line shape changes as crystallization progresses. For clarity, only some of the spectra are displayed, namely those measured at fixed time intervals (specified in minutes in each panel).

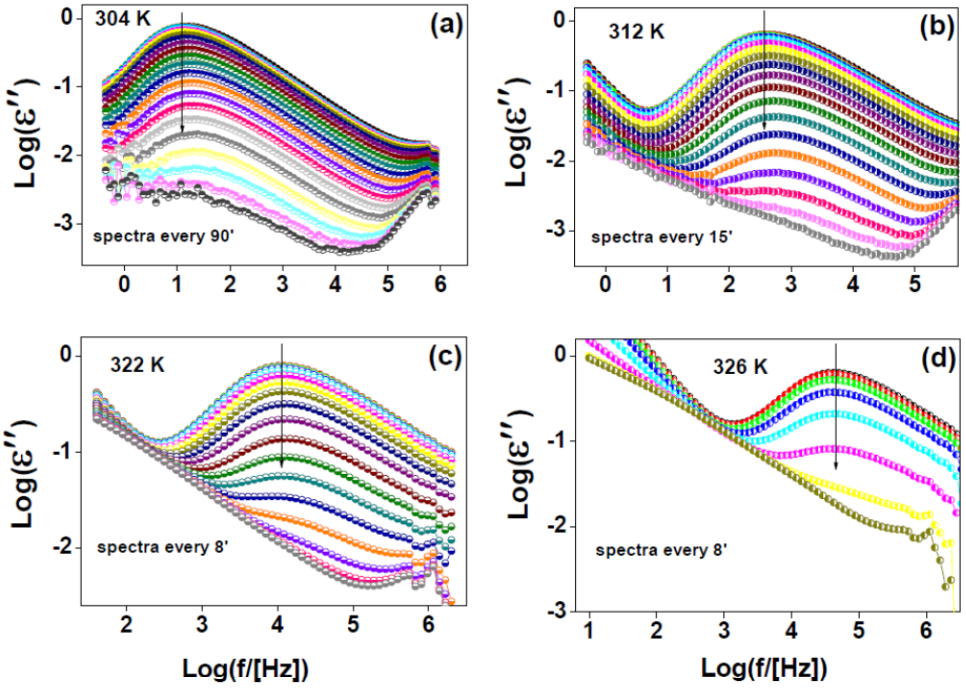

Figure 4. Loss spectra ε″(*f*) of Biclotymol during isothermal measurements at 304 (a), 312 (b), 322 (c) and 326 K (d). The strength of the loss feature, proportional to the number of molecules in the amorphous phase, decreases over time due to crystallization (see arrows). The displayed spectra

correspond to the same measurements as in Figure 3, namely those acquired at fixed time intervals as specified in each panel.

After nucleation of the metastable Phase II, and during its growth, the sample is in a mixed phase that is partially crystalline and partially amorphous. Figure 5(a) shows an optical microscopy image of the sample taken during the crystallization process. Needle-like (Phase II) crystallites are observed, which are embedded in an amorphous (supercooled liquid) Biclotymol matrix from which they are spontaneously nucleated.

The fits of the series of loss spectra shown in Figure 4 indicate that, as the dielectric strength of the α relaxation decreases during isothermal annealing, it also shifts slightly towards larger frequencies. In other words, the time τ_α of maximum loss of the amorphous part of the sample becomes shorter during the growth of the crystallites, as visible in Figure 5(b). The origin of such shift must be related to the growth of the crystallites at the expense of the amorphous phase. One possibility is that (partial) crystallization results in smaller amorphous domains in which the cooperative α process involves dynamically-correlated clusters of fewer molecules, thus yielding faster dynamics. Another possibility is that, since the density of a crystal phase is usually higher than that of the amorphous phase, partial crystallization results in a larger free volume per molecule in the amorphous state (to put it in different words, the molecular dynamics is faster at the surface of a cluster where the molecules have lower coordination number, and such "surface effect" becomes more important as the size of amorphous domains is reduced). At the same time, the width of the relaxation feature increased (as visible e.g. in the increase of the shape parameter *p* over time, not shown). This is indicative of a greater variety of local environments of the Biclotymol molecules in the amorphous phase as the crystallization progresses, and it likely results from the shrinking of amorphous domains, which leads to different extent and shape of cooperatively relaxing molecular clusters (more pronounced surface/interface effect). A spectral evolution of the α relaxation peak during crystallization is frequently observed (Jiménez-Ruiz *et al*, 2002; Sanz *et al*, 2004).

The evolution of the spectral strength $\Delta\varepsilon$ is best observed in the real permittivity spectra (Figure 3), where it corresponds to the difference between the static permittivity value ε_s at the lowest frequencies (*i.e.*, between 0.1 and 100 Hz depending on the measuring temperature) and the value ε_∞ at frequencies higher than that of the relaxation peak (*e.g.*, at the highest measured frequency of $2 \cdot 10^6$ Hz). The initially constant value of ε_s observed in the series of isothermal spectra acquired at 304 or 312 K corresponds to the full dielectric strength in the supercooled liquid phase before the onset of crystallization. As mentioned above, the quantity $\Delta\varepsilon = \varepsilon_s - \varepsilon_\infty$ is directly proportional to the number of molecules in the amorphous phase, so that $\Delta\varepsilon$ decreases as the crystallization develops.

To analyze the crystallization kinetics, we have studied the time evolution of the normalized static-permittivity difference, defined as (D'Amore *et al*, 1990):

(Eq. 6) $\hat{\varepsilon}(t) = \frac{\varepsilon_s(t) - \varepsilon_s(\mathrm{SL})}{\varepsilon_s(\mathrm{MC}) - \varepsilon_s(\mathrm{SL})}$

Here ε_s(SL) and ε_s(MC) are the static permittivity of the supercooled liquid and metastable crystal (Phase II), respectively, as measured the former before the onset of nucleation of the crystal phase

and the latter at the end of the crystal growth, while $\varepsilon_s(t)$ is the static permittivity of the mixed-phase sample as a function of the time elapsed from the start of the isothermal measurements. The quantity $\hat{\varepsilon}(t)$ is plotted in Figure 5(c) for all four studied crystallization temperatures. For small t, the sample is still in the supercooled liquid state and $\varepsilon_s(t) = \varepsilon_s(\mathrm{SL})$, so that $\hat{\varepsilon} = 0$, while for large t the sample has crystallized completely and $\varepsilon_s(t) = \varepsilon_s(\mathrm{MC})$, so that $\hat{\varepsilon} = 1$ (these lower and upper bounds are indicated by dashed lines in Figure 5(c)).

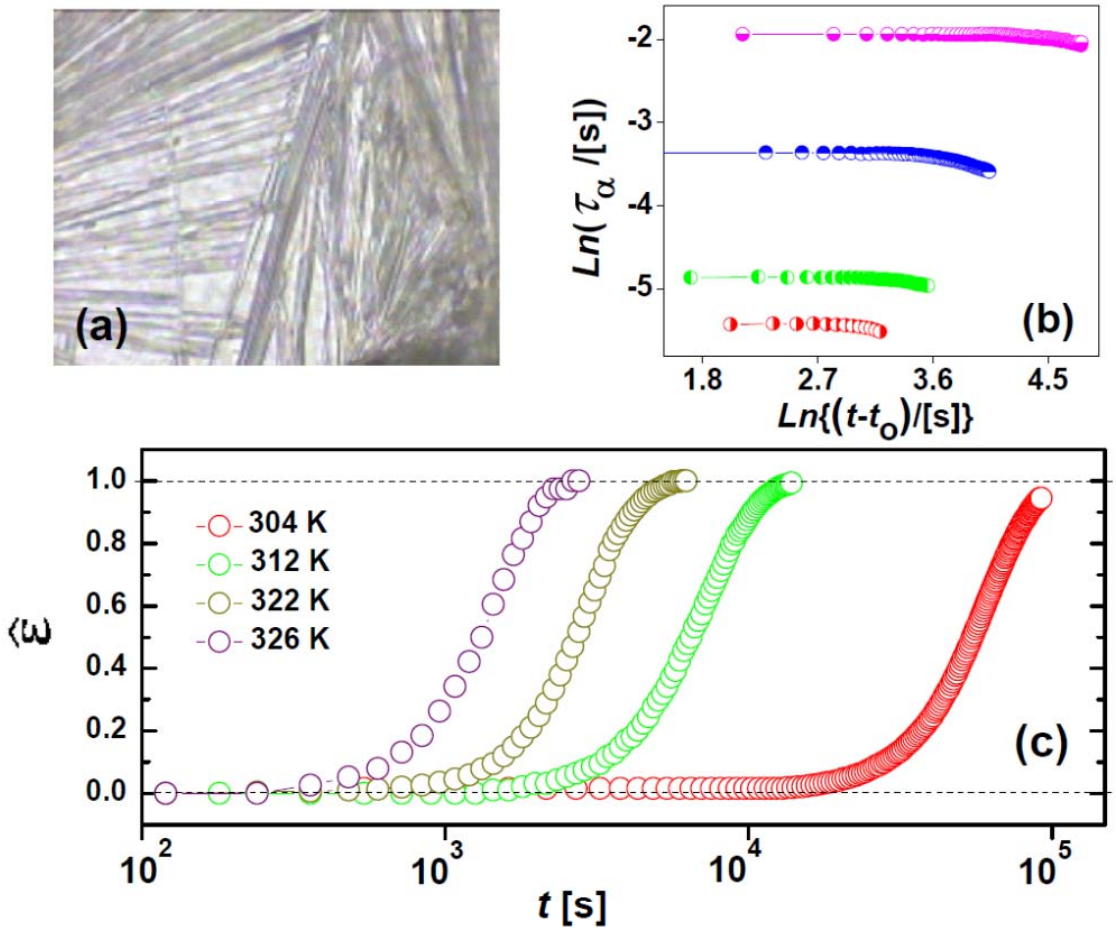

Figure 5. (a) Optical microscopy photograph of the needle-like crystallites of Phase II of Biclotymol grown spontaneously from the supercooled liquid state. (b) Logarithmic plot of the time-evolution of the characteristic relaxation time τ_α of the α relaxation, during crystallization from the supercooled liquid phase to the crystalline Phase II of Biclotymol, as a function of time since the induction time t_o. (c) Time evolution of the normalized static-permittivity difference $\hat{\varepsilon}$ during crystallization, as a function of the time elapsed since the start of each isothermal measurement (in logarithmic scale). Both τ_α and $\hat{\varepsilon}$ are plotted as a function of time for all four isothermal crystallization temperatures (304, 312, 322 and 326 K).

The normalized static-permittivity difference can be used to describe the time-dependence of the crystallization process, *i.e.*, the crystallization kynetics. Assuming an Avrami-like temporal dependence of the crystallization (Avrami, 1939; Avrami, 1940), the normalized static-permittivity difference can be described by the equation (Adrjanowicz et al, 2010):

(Eq. 7) $\hat{\varepsilon}(t) = 1 - \exp(-K(t - t_o)^n)$

In this expression, valid at times greater than the induction time t_o (onset time of nucleation of the crystal phase), *K* is the temperature-dependent crystallization rate and *n* is the so-called Avrami exponent, which depends only on the crystal morphology and crystallization mechanism (Wunderlich, 1976; see also below). To verify the dependence predicted by Eq. (7), in Figure 6 we have plotted the quantity $Ln[-Ln(1-\hat{\varepsilon})]$ versus $Ln(t - t_o)$ (Avrami plot) for all four studied temperatures. It may be observed that for all the temperatures studied the crystallization kinetics follows the time dependence predicted by the Avrami equation, with virtually the same slope (*i.e.*, the same exponent *n*). The best-fit parameters obtained by fitting the experimental data to Eq. 7 are shown in Table 1, together with the experimental values of the induction time t_o. The crystallization rate *K* and the induction time t_o are displayed as Arrhenius plots in the inset to Figure 6.

T (K)	t_o (min)	$Ln(K)$	n
304 ± 0.1	295 ± 2	-9.66 ± 0.03	2.00 ± 0.01
312 ± 0.1	26 ± 2	-7.92 ± 0.04	2.01 ± 0.01
322 ± 0.1	13 ± 2	-7.22 ± 0.05	2.04 ± 0.02
326 ± 0.1	4 ± 2	-6.96 ± 0.14	2.14 ± 0.05

Table 1. Experimental parameters obtained by fitting the experimental normalized static-permittivity difference by means of the Avrami equation, Eq. (7), together with the induction time t_o (time elapsed before the crystallization onset).

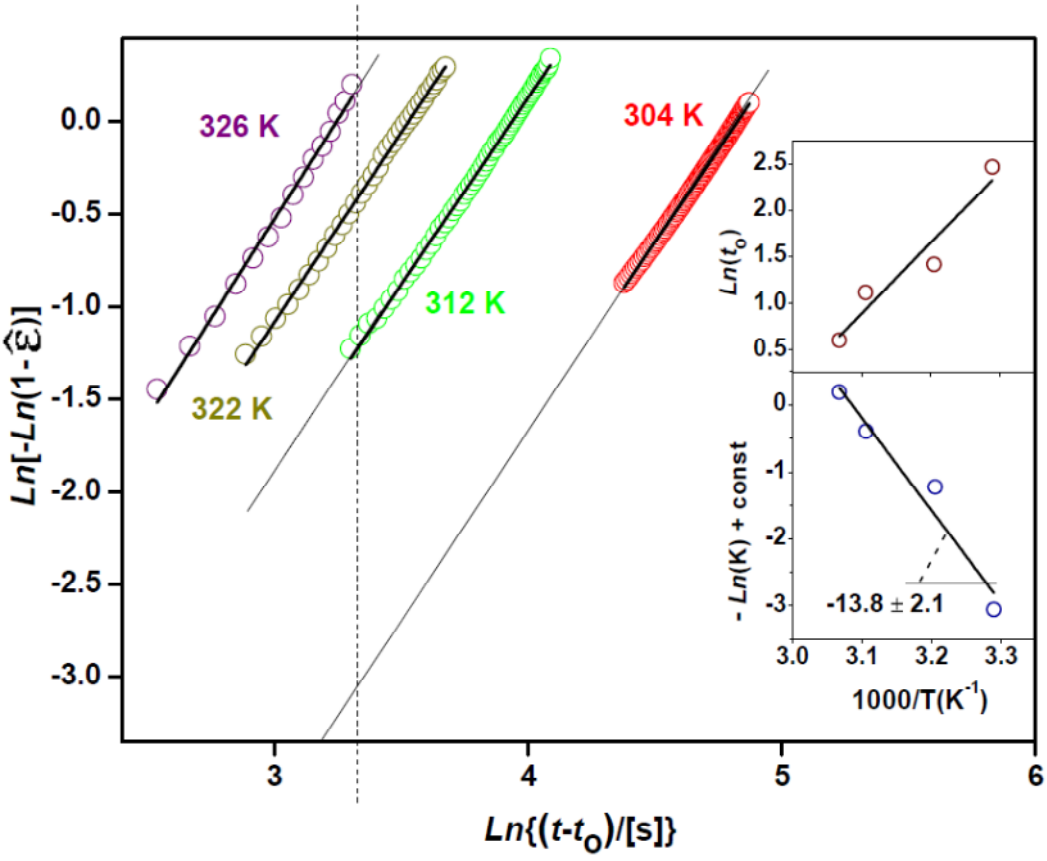

Figure 6. Avrami plot of the normalized static-permittivity difference $\hat{\varepsilon}$ as a function of the time elapsed from the crystallization onset ($t - t_o$), for all four isothermal crystallization temperatures studied. The continuous lines are linear fits, while the dashed vertical line indicates the time at which the value of the ordinate was taken for calculating the activation barrier of the crystallization process. The corresponding ordinate values are shown as an Arrhenius plot in the bottom inset (see the text for more details), while the top inset shows the Arrhenius plot of the induction time t_o.

It may be observed that the induction time t_o decreases with increasing temperature, and that the crystallization rate increases with temperature. Both features are expected since higher temperature implies higher thermal energy and therefore higher probability that the crystal phase may nucleate and grow. Though nucleation and growth are independent processes, both processes are boosted by a temperature increase, as visible from the insets to Figure 6. In principle, the induction time should correlate only with the nucleation rate, while the crystallization rate *K* depends both on the nucleation rate and on the growth rate. The crystallization rate *K* is expected to display a simply-activated thermal behavior, that is, to scale as (Málek, 2000):

(Eq. 8) $Ln[K(T)] \sim -\frac{E_a}{k_B T}$

In this expression, $k_B T$ is the thermal energy and E_a is the activation barrier for the crystallization process. The crystallization rates reported in Table 1 correspond to the intercept of the Avrami plots of Figure 6, *i.e.* to the value of the fit function when the abscissa is zero. Because this extrapolated value is far from the experimental data points, it can be strongly affected by an error in the determination of the slope. For this reason, to study the temperature dependence of *Ln*(*K*) we have taken the value of the fit function at the time t^* given by $Ln(t^* - t_o) = 3.329$ (marked by the dashed vertical line in Figure 6), time at which experimental values are available for three out of the fours studied temperatures. If, as supported by of Figure 6, the slope of all four Avrami plots is the same, then the vertical separation between them is independent of time (value of the abscissa), so that any value of the abscissa can be used to track the temperature dependence of the crystallization rate. The values thus obtained are shown as Arrhenius plot in the bottom inset to Figure 6. The obtained points were fitted assuming a simply-activated behavior. The value of the activation energy extracted from the slope of such linear fit was $E_a = 115 \pm 22$ kJ mol^{-1}. A similar value (but with a higher percent uncertainty) is obtained from the Arrhenius-law fit of the values of *Ln*(*k*) listed in Table 1. Also the induction time appears to follow an activated behavior, as visible in the top inset to Figure 6, albeit with a different activation energy, as expected.

It may be observed in Table 1 that, while both t_o and *K* are clearly temperature-dependent, the value of *n* is basically constant for all studied temperatures. This is also visible from the very similar slopes of all four Avrami plots in Figure 6. The Avrami exponent is indeed expected to have a fixed value because it depends only on the crystallite morphology and growth mechanism (Wunderlich, 1976), and these features are not expected to change in a relatively narrow temperature interval as the one studied here. It may be observed from Figure 6 that for the temperature of T = 326 K, where crystallization is quite fast, the agreement between the fewer experimental points available and the Avrami model is less than optimal, which is possibly due to the fact that at high crystalline volume fraction deviations from the Avrami law can occur due to boundary effects (Schaafsma *et al*, 1979).

If we exclude the value of *n* found for such temperature, then the value of the Avrami exponent for Biclotymol is obtained as $n = 2.02 \pm 0.02$.

Avrami's original theory concerned homogeneous crystallization in 1, 2 or 3 dimensions, and predicted an integer value of *n* between 1 and 4 (Avrami, 1939; Avrami, 1940). As visible in Figure 5(a), the metastable Phase II grows into needle-like crystallites, *i.e.*, it displays a typically one-dimensional growth. Such long and thin crystallites appear to nucleate at different times after the induction time t_o (they display different length at different elapsed times) and to grow forming bundles (Schammé *et al*, 2015; Céolin *et al*, 2008). The exponent $n = 2$ corresponds then to one-dimensional (needle-like) crystallization with a continuous, time-independent nucleation rate after the onset time t_o (Çelikbilek *et al*, 2012). Biclotymol appears to be a textbook-like example of the integer Avrami law for crystal nucleation and growth.

Conclusions

We have presented a dielectric spectroscopy study of the relaxation dynamics and crystallization kinetics in the supercooled amorphous phase of the pulmonary antiseptic Biclotymol. This pharmaceutically active molecule is found to be a relatively fragile glass-former with fragility index $m = 86 \pm 13$. The primary relaxation process is characterized by an asymmetric spectral lineshape and non-simply-activated temperature dependence. This collective relaxation freezes out at the glass transition temperature of $T_g = 290 \pm 1$ K. Also a secondary relaxation feature is observed near and below T_g. This secondary relaxation, which exhibits simply-activated thermal behavior with activation energy of 75.5 ± 0.7 kJ mol^{-1}, corresponds to an intramolecular dynamic process likely associated with hydrogen bonding. No clear precursor (Johari–Goldstein) relaxation could be observed, which could explain the reported stability of amorphous Biclotymol a few degrees above T_g, where the collective dynamics is almost frozen while the secondary relaxation is not. The crystallization mechanism is one-dimensional, with a constant rate of nucleation and growth, leading to the formation of needle-like crystallites and to an Avrami exponent equal to 2, which is found to be independent of temperature. The activation barrier for crystallization is 115 ± 22 kJ mol^{-1}, a value similar to that of other low-mass organic molecules and active pharmacological ingredients. Our study shows that dielectric spectroscopy characterization is a valuable tool to investigate and understand the kinetic stability of amorphous pharmaceuticals.

Abbreviations

VFT: Vogel–Fulcher–Tammann

Acknowledgments

This work has been partially supported by the Spanish Ministry of Science and Innovation through project FIS2014-54734-P and by the Generalitat de Catalunya under project 2014 SGR-581.

References

(Adrjanowicz *et al*, 2010) Adrjanowicz, K.; Kaminski, K.; Wojnarowska, Z.; Dulski, M.; Hawelek, L.; Pawlus, S.; Paluch, M. *J. Phys. Chem. B* **2010**, 114, 6579–6593. (DOI: 10.1021/jp910009b)

(Adrjanowicz *et al*, 2012a) Adrjanowicz, K.; Kaminski, K.; Paluch, M.; Ngai, K.L.; Yu L. Study of dynamics and crystallization kinetics of 5-methyl-2-[(2-nitrophenyl)amino]-3-thiophenecarbonitrile at ambient and elevated pressure. *J. Chem. Phys.* **2012**, 136, 234509. (DOI: 10.1063/1.4728162)

(Adrjanowicz *et al*, 2012b) Adrjanowicz, K.; Zakowiecki, D.; Kaminski, K.; Hawelek, L.; Grzybowska, K.; Tarnacka, M.; Paluch, M.; Cal, K. Molecular Dynamics in Supercooled Liquid and Glassy States of Antibiotics: Azithromycin, Clarithromycin and Roxithromycin Studied by Dielectric Spectroscopy. Advantages Given by the Amorphous State. *Mol. Pharmaceutics* **2012**, 9, 1748−1763. (DOI: 10.1021/mp300067r)

(Alvarez *et al*, 1991) Alvarez, F.; Alegra, A.; Colmenero, J. Relationship between the time-domain Kohlrausch-Williams-Watts and frequency-domain Havriliak-Negami relaxation functions. *Phys. Rev. B* **1991**, 44, 7306–7312. (DOI: 10.1103/PhysRevB.44.7306)

(Alvarez *et al*, 1993) Alvarez, F.; Alegra, A.; Colmenero, J. Interconnection between frequency-domain Havriliak-Negami and time-domain Kohlrausch-Williams-Watts relaxation functions. *Phys. Rev. B* **1993**, 47, 125–130. (DOI: 10.1103/PhysRevB.47.125)

(Angell 1988) Angell, C.A. Structural instability and relaxation in liquid and glassy phases near the fragile liquid limit. *J. Non-Cryst. Solids* **1988**, 102, 205−221. (DOI: 10.1016/0022-3093(88)90133-0)

(Avrami, 1939) Avrami, M. Kinetics of Phase Change. I. General Theory. *J. Chem. Phys.*, **1939**, 7, 1103−1112. (DOI: 10.1063/1.1750380)

(Avrami, 1940) Avrami, M. Kinetics of Phase Change. II Transformation-Time Relations for Random Distribution of Nuclei. *J. Chem. Phys.* **1940**, 8, 212−224. (DOI: 10.1063/1.1750631)

(Bhardwaj *et al*, 2013) Bhardwaj, S.; Arora, K.; Kwong, E.; Templeton, A.; Clas, S.D.; Suryanarayanan, R. Correlation between Molecular Mobility and Physical Stability of Amorphous Itraconazole. *Mol. Pharmaceutics* **2013**, 10, 694−700. (DOI: 10.1021/mp300487u)

(Böhmer *et al*, 1993) Böhmer, R.; Ngai, K.L.; Angell, C.; Plazek, D. Nonexponential relaxations in strong and fragile glass formers. *J. Chem. Phys.* **1993**, 99, 4201−4209. (DOI: 10.1063/1.466117)

(Capaccioli *et al*, 2007) Capaccioli, S.; Ngai, K.L.; Shinyashiki, N. The Johari-Goldstein β-Relaxation of Water. *J. Phys. Chem. B* **2007**, 111, 8197–8209. (DOI: 10.1021/jp071857m)

(Capen *et al*, 2012) Capen, R.; Christopher, D.; Forenzo, P.; Ireland, C.; Liu, O.; Lyapustina, S.; O'Neill, J.; Patterson, N.; Quinlan, M.; Sandell, D.; Schwenke, J.; Stroup, W.; Tougas, T. On the Shelf Life of Pharmaceutical Products. *AAPS PharmSciTech*. **2012**, 13, 911–918. (DOI: 10.1208/s12249-012-9815-2)

(Céolin *et al*, 2008) Céolin, R.; Tamarit, J. Ll; Barrio, M.; Lopez, D.O.; Nicolaï, B.; Veglio, N.; Perrin, M.; Espeau, P. Overall Monotropic Behavior of a Metastable Phase of Biclotymol, 2,2'-Methylenebis(4-Chloro-3-Methyl-Isopropylphenol), Inferred From Experimental and Topological Construction of the Related P-T State Diagram. *J. Pharm. Sci.* **2008**, 97, 3927−3941. (DOI: 10.1002/jps.21285)

(Çelikbilek *et al*, 2012) Çelikbilek, M.; Ersundu, A. E.; Aydın, S. Crystallization Kinetics of Amorphous Materials. In: *Advances in crystallization processes*, **2012**, Ch. 6

(Colmenero *et al*, 1997) Colmenero, J. ; Arbe, A. ; Coddens, G. ; Frick, B. ; Mijangos, C. ; Reinecke, H. Crossover from Independent to Cooperative Segmental Dynamics in Polymers: Experimental Realization in Poly(Vinyl Chloride). *Phys. Rev. Lett.* **1997**, 78, 1928–1931. (DOI : 10.1103/PhysRevLett.78.1928)

(D'Amore *et al*, 1990) D'Amore, A.; Kenny, J. M.; Nicolais, L.; Tucci, V. Dynamic-mechanical and dielectric characterization of PEEK crystallization. *Polym. Eng. Sci*. **1990**, 30, 314–320. (DOI: 10.1002/pen.760300509)

(Ediger *et al*, 2008) Ediger, M. D.; Harrowell, P.; Yu, L. Crystal Growth Kinetics Exhibit a Fragility-Dependent Decoupling from Viscosity. *J. Chem. Phys.* **2008**, 128, 034709–034714. (DOI: 10.1063/1.2815325)

(Gupta *et al*, 2004) Gupta, P.; Chawla, G.; Bansal, A. Physical Stability and Solubility Advantage from Amorphous Celecoxib: The Role of Thermodynamic Quantities and Molecular Mobility. *Mol. Pharmaceutics* **2004**, 1, 406−413. (DOI: 10.1021/mp049938f)

(Havriliak and Negami, 1966) Havrilliak S.; Negami, S. A complex plane analysis of α-dispersions in some polymer systems. *J. Polym. Sci.-Pt. C* **1966**, 16, 99−117. (DOI: 10.1002/polc.5070140111)

(Havriliak and Negami, 1967) Havrilliak S.; Negami, S. A complex plane representation of dielectric and mechanical relaxation processes in some polymers. *Polymer* **1967**, 8, 161−210. (DOI: 10.1016/0032-3861(67)90021-3)

(Hensel-Bielowka *et al*, 2005) Hensel-Bielowka, S.; Paluch, M.; Ngai, K.L. *J. Chem. Phys.*, **2005**, 123, 014502. (DOI: 10.1063/1.1946752)

(Jiménez-Ruiz *et al*, 2002) Jiménez-Ruiz, M.; Ezquerra, T. A.; Sics, I.; Fernández-Díaz. Crystallization of 2-propanol studied by neutron diffraction and dielectric spectroscopy in real-time. *M. T. Appl. Phys. A* **2002**, 74 (Suppl. 1), S543−S545. (DOI: 10.1007/s003390101119)

(Johari and Goldstein, 1970) Johari, G.P.; Goldstein, M. Viscous Liquids and the Glass Transition. II. Secondary Relaxations in Glasses of Rigid Molecules. *J. Chem. Phys.* **1970**, 53, 2372–2388. (DOI: 10.1063/1.1674335)

(Kaminski *et al*, 2011) Kaminski, K.; Adrjanowicz, K.; Wojnarowska, Z.; Dulski, M.; Wrzalik, R.; Paluch, M.; Kaminska, E.; Kasprzycka, A. Do Intermolecular Interactions Control Crystallization Abilities of Glass-Forming Liquids? *J. Phys. Chem. B* **2011**, 115, 11537–11547. (DOI: 10.1021/jp202368b)

(Kremer and Schönhals, 2003) Kremer F.; Schönhals A. *Broad Band Dielectric Spectroscopy*, Springer, Berlin, **2003,** Ch. 3 and 4.

(Macovez *et al*, 2014) Macovez, R.; Mitsari, E.; Zachariah, M.; Romanini, M.; Zygouri, P.; Gournis, D.; Tamarit, J.Ll. Ultraslow Dynamics of Water in Organic Molecular Solids. *J. Phys. Chem. C* **2014**, 118, 4941−4950. (DOI: 10.1021/jp4097138)

(Málek, 2000) Málek, J. Kinetic analysis of crystallization processes in amorphous materials *Themochimica Acta* **2000**, 355, 239−253. (DOI: 10.1016/S0040-6031(00)00449-4)

(Ngai, 1998) Ngai, K.L. Relation between some secondary relaxations and the α relaxations in glass-forming materials according to the coupling model. *J. Chem. Phys.* **1998**, 109, 6982–6994. (DOI: 10.1063/1.477334)

(Ngai, 2007) Ngai, K.L. Why the glass transition problem remains unsolved? *J. Non-Cryst. Solids* **2007**, 353, 709–718. (DOI: 10.1016/j.jnoncrysol.2006.12.033)

(Ngai and Paluch, 2004) Ngai, K.L.; Paluch, M. Classification of secondary relaxation in glass-formers based on dynamic properties. *J. Chem. Phys.* **2004**, 120, 857–873. (DOI: 10.1063/1.1630295)

(Patterson *et al*, 2005) Patterson, J.; James, M.; Forster, A.; Lancaster, R.; Butler, J.; Rades, T. The Influence of Thermal and Mechanical Preparative Techniques on the Amorphous State of Four Poorly Soluble Compounds. *J. Pharm. Sci.* **2005**, 94, 1998–2012. (DOI: 10.1002/jps.20424)

(Pogna *et al*, 2015) Pogna, E.A.A.; Rodriguez-Tinoco, C.; Cerullo, G.; Ferrante, C.; Rodriguez-Viejo, J.; Scopigno, T. Probing equilibrium glass flow up to exapoise viscosities. *Proc. Natl. Acad. Sci. U.S.A.* **2015**, 112, 2331–2336. (DOI: 10.1073/pnas.1423435112)

(Sanz *et al*, 2004) Sanz, A.; Jiménez-Ruiz, M.; Nogales, A.; Martín y Marero, D.; Ezquerra, T. A. Hydrogen-Bond Network Breakage as a First Step to Isopropanol Crystallization. *Phys. Rev. Lett.* **2004**, 93, 015503. (DOI:10.1103/PhysRevLett.93.015503)

(Schaafsma *et al*, 1979) Schaafsma, A.S.; Snijders, H.; van der Woude, F.; Drijver, J.W.; Radelaar, S. Amorphous to crystalline transformation of $Fe_{80}B_{20}$. *Phys. Rev. B* **1979**, 20, 4423–4430. (DOI: 10.1103/PhysRevB.20.4423)

(Schammé *et al*, 2015) Schammé, B.; Couvrat, N.; Malpeli, P.; Delbreilh, L.; Dupray, V.; Dargent, É.; Coquerel, G. Crystallization Kinetics and Molecular Mobility of an Amorphous Active Pharmaceutical Ingredient: a Case Study with Biclotymol. *Int. J. Pharm*. **2015**, 490, 248−257. (DOI: 10.1016/j.ijpharm.2015.05.036)

(Serajuddin, 1999) Serajuddin, A. Solid Dispersion of Poorly Water-Soluble Drugs: Early Promises, Subsequent Problems, and Recent Breakthroughs. *J. Pharm. Sci.* **1999**, 88, 1058−1066. (DOI: 10.1021/js980403l)

(Wunderlich, 1976) Wunderlich, B. Macromolecular Physics. Crystal Nucleation, Growth, Annealing. Academic Press: London, **1976**; Vol. 2

(Yu, 2001) Yu, L. Amorphous pharmaceutical solids: preparation, characterization and stabilization. *Adv. Drug Deliv. Rev.* **2001**, 48, 27–42. (DOI: 10.1016/S0169-409X(01)00098-9)

(Zhou *et al*, 2002) Zhou, D.; Zhang, G.; Law, D.; Grant, D.; Schmitt, E. Physical Stability of Amorphous Pharmaceuticals: Importance of Configurational Thermodynamic Quantities and Molecular Mobility. *J. Pharm. Sci.* **2002**, 91, 1863–1872. (DOI: 10.1002/jps.10169)